IEEJ TRANSACTIONS ON ELECTRICAL AND ELECTRONIC ENGINEERING
IEEJ Trans 2013; **8**: 7–18
Published online in Wiley Online Library (wileyonlinelibrary.com). DOI:10.1002/tee.21785

Paper

Comprehensive Comparison of FACTS Devices for Exclusive Loadability Enhancement

Arthit Sode-Yome*[a], Non-member
Nadarajah Mithulananthan**, Non-member
Kwang Y. Lee***, Non-member

A complete comparison of a number of well-known flexible alternating current transmission system (FACTS) devices for static voltage stability enhancement is presented. Various performance measures including power–voltage ($P-V$) curves, voltage profiles, and power losses are compared under normal and contingency conditions. The importance of proper modeling of FACTS devices, including the DC side, is emphasized because, at their limits, most of these devices behave like a fixed capacitor or inductor. A simple placement technique of series FACTS devices and unified power flow controller (UPFC) is proposed considering exclusive loading margin enhancement. A new idea of loading margin increase per cost is proposed to find the appropriate FACTS devices for investment. The paper provides a guide for utilities to have an appropriate choice of FACTS device for enhancing static voltage stability and loading margin by comparing technical merits and demerits of each of these devices in terms of system performance. © 2012 Institute of Electrical Engineers of Japan. Published by John Wiley & Sons, Inc.

Keywords: FACTS devices, loadability, static voltage stability, placement technique

Received 9 November 2010; Revised 9 September 2011

1. Introduction

Voltage instability has been a major threat in power systems. Voltage instability that could lead to widespread blackout is more severe in large interconnected power systems compared to small individual systems. The whole country or an entire state could get stranded as a result of blackout due to voltage instability, and the associated losses, both monetary and non-monetary, could be substantial [1–3]. This phenomenon is more pronounced in the current electricity market scenario as power systems will be operating under more stressed conditions due to profit or social welfare maximization objective. Hence, it is important for electric power utilities or independent system operators (ISOs) around the world to do a thorough investigation on the voltage stability on their systems by taking into account the neighboring interconnections as well. Here, the fundamental question is whether the systems have enough loading margin (LM) even with some credible contingency. If there is enough margin with credible contingency, the problem of voltage instability could be avoided.

Though there are a number of factors directly or indirectly influencing dynamic and static voltage instability, the fundamental reason of this problem is lack of reactive power reserve [4–7,8]. Unlike real power, reactive power is easy to produce but difficult to transfer. The challenge here would be to provide adequate reactive power support at the appropriate location whenever it is needed. Traditionally, reactive power has been produced by capacitors because this way of producing reactive power is considered the cheapest solution. However, capacitors are unable to smoothly control their reactive power output which varies in proportion to the square of the terminal voltage to which they are connected. That leads to the development and deployment of devices popularly known as flexible alternating current transmission systems (FACTS) devices. These devices can provide dynamic reactive power in a smooth way unlike the capacitors.

Among various types of FACTS devices, static variable compensator (SVC), static synchronous compensator (STATCOM), thyristor-controlled series capacitor (TCSC), static synchronous series compensator (SSSC), and unified power flow controller (UPFC) are well known [9]. Each of these FACTS devices, however, has its own characteristics and limitations [9–11]. Some of these devices, namely STATCOM, SSSC, and UPFC, could be considered as new-generation FACTS devices as they are based on voltage source converters (VSCs). In this group, there are no capacitor or thyristor-controlled reactors (TCRs) as such; however, the capacitive and inductive effects are realized by appropriate control of the VSC. These devices are expected to perform better compared to the traditional counter parts, namely SVC and TCSC. As these devices defer in cost and construction, it would be useful to study and compare the well-known FACTS devices, namely SVC, STATCOM, TCSC, SSSC, and UPFC.

Appropriate models of these FACTS devices, including both AC and DC sides, are required to accurately capture their behaviors when they are operating at their limits. Moreover, as in the case of dynamic stability, optimal placement and sizing of these FACTS devices are important issues [12,13]. Placing appropriate FACTS device at suitable locations with proper sizes would lead to maximum LM for static voltage stability. In Ref. [14], detailed steady-state models with control of SVC and TCSC to study their effects on voltage collapse phenomena in power systems are presented. Furthermore, Ref. [15] proposes AC/DC models for representing the UPFC for load flow and transient stability studies. In Ref. [11], transient stability and power flow models of

[a] Correspondence to: Arthit Sode-Yome. E-mail: arthit@ieee.org

* Department of Electrical Engineering, Siam University, Bangkok 10163, Thailand

** School of Information Technology and Electrical Engineering, University of Queensland, Brisbane, Australia

*** Department of Electrical and Computer Engineering, Baylor University, Waco, TX 76798-7356, USA

SVC, STATCOM, TCSC, SSSC, and UPFC suitable for voltage and angle stability studies are presented. In addition, Ref. [10] compares a shunt capacitor, SVC, and STATCOM in static voltage stability improvement.

Very scant research attention has been paid on AC/DC models of FACTS devices, especially VSC-based ones, in static voltage stability study as the DC side representation is important in sizing and accurately representing the limits of these devices. This could provide more accurate reflections of FACTS devices under stressed system conditions, especially when the devices are operating at their limits. The study should also compare all available FACTS devices in terms of voltage stability margin in the same system to rank them based on their performances and cost. This would be useful for utilities who would like to invest in FACTS devices to select the most appropriate FACTS device in the context of static voltage stability. The merits and demerits of all FACTS devices could also be revealed with regard to voltage stability.

Based on the above observation, attention is drawn in this paper to study the influence of well-known FACTS devices on static voltage stability. AC/DC model is used to represent AC and DC characteristics of VSC-based FACTS devices.

The rest of the paper is structured as follows: Section 2 summarizes concepts of static voltage stability. Section 3 presents structures and models of well-known FACTS devices. Siting and sizing issues of FACTS for loadability enhancement are addressed in Section 4. Test system along with analysis tools used and numerical results and discussion are presented in Section 5. Finally, in Section 6, a summary of the main conclusions and contributions of the paper is presented.

2. Loadability

2.1. Loadability Static voltage instability is mainly associated with reactive power imbalance. Reactive power support that the bus receives from the system can limit loadability of that bus and hence the entire system. If the reactive power support reaches the limit, usually the maximum limit, the system will approach the maximum loading point or voltage collapse point due to high real and reactive power losses due to transmission of real and reactive power [2,4,10,14]. In order to minimize this, at least the reactive power support should be local.

In static voltage stability, slowly developing changes in the power system occur that eventually lead to a shortage of reactive power and declining voltage. This phenomenon can be seen from the plot of the voltage at receiving end versus the power transferred. The plots are popularly referred to as power–voltage (P–V) curve or 'nose' curve. As the power transfer increases, the voltage at the receiving end decreases. Eventually, the critical (nose) point, the point at which the system reactive power is depleted, is reached where any further increase in the active power transfer will lead to a very rapid decrease in the magnitude of the voltage. Before reaching the critical point, a large voltage drop due to heavy reactive power losses can be observed. The maximum load that can be supplied prior to the point at which the system reactive power is depleted is called the *static voltage stability margin* or *loading margin* (LM) of the system. It is also widely known as the *loadability* of the system.

2.2. Modeling The power flow model is used to investigate static voltage stability because the power flow equation yields adequate results, as singularities in related power flow Jacobian can be associated with actual singular bifurcation of the corresponding dynamical system [2]. The power flow model is represented by

$$F(z,\lambda) = \begin{bmatrix} \Delta P(z,\lambda) \\ \Delta Q(z,\lambda) \end{bmatrix} = 0 \tag{1}$$

where $F(z, \lambda)$ is power flow equation and λ is the loading factor (LF) or system load change that drives the system to collapse in the following way:

$$\begin{aligned} P_{D,i} &= P_{Do,i}(1 + \lambda K_{P,i}) \\ Q_{D,i} &= Q_{Do,i}(1 + \lambda K_{Q,i}) \end{aligned} \tag{2}$$

where $P_{Do,i}$ and $Q_{Do,i}$ represent the initial active and reactive loads at bus i, and constants K_{Pi} and K_{Qi}, respectively, represent the active and reactive load increase direction of bus i.

2.3. Analysis techniques The purposes of analysis techniques are to identify system conditions causing voltage instability, to find LM of the system, and to specify the parameters affecting the voltage stability of the system. In static voltage stability study, four analysis techniques are popularly used, namely, direct, modal analysis, continuation power flow (CPF), and optimization technique methods.

2.3.1. Direct method Direct method uses power flow equations, singular conditions of the power flow Jacobian, and nonzero left eigenvectors to find the maximum loading point. An obvious disadvantage of this technique is the high computational cost, requiring good initial conditions. In addition, pertinent information between maximum LM and the base case is not available.

2.3.2. Modal analysis method In standard power flow, the Jacobian contains the first derivatives of the reactive power mismatch equation with respect to the voltage magnitude V. The load flow Jacobian can be decomposed into left and right eigenvector matrices and the matrix of singular values. The singularity of system Jacobian can be used as an indicator to detect the proximity of voltage instability. Moreover, right and left eigenvectors, which are the decomposition of the Jacobian, can reveal information related to the weakest bus and the weakest area of the system.

2.3.3. Continuation power flow (CPF) method The CPF method uses the successive power flow solution to fully compute the voltage profiles up to collapse point to determine the LM. It involves predictor and corrector steps to guarantee a well-behaved numerical solution of the related equation. The method is an iterative method that can trace P–V curve of the system up to the maximum loading ('nose') point without having numerical problems. P–V curves are currently in use at some utilities for determining proximity to collapse so that the operator can take timely preventive measures to avoid voltage collapse.

2.3.4. Optimization method Static voltage stability study can be carried out by maximizing the LF subject to power flow equations. Optimization technique such as Lagrangian multipliers can be used to find the necessary conditions. These necessary conditions are identical to those obtained from the direct method with the exception of one equation that guarantees nonzero left eigenvectors. Other power system limits, such as voltage and thermal limits, can also be introduced in the optimization formulation as inequality constraints.

Voltage instability of the system can be avoided by increasing the voltage stability margin. This margin can be enhanced by various ways, i.e. by adding reactive power sources, increasing generation at the appropriate locations, or reducing reactive power losses throughout the system. Introducing FACTS devices at the appropriate location, where the reactive power support is needed the most, is an effective way to increase the voltage stability margin. It can be also viewed as a way to reduce reactive power losses, as the power flow is changed to less congested lines. In the following section, the concepts and structures of well-known FACTS devices used in this paper are presented.

Table I. Cost comparison of capacitors and FACTS controllers

Conventional devices/FACTS controller	Cost (USD)
Shunt capacitor	8/kVar
Series capacitor	20/kVar
SVC	40/kVar controlled portions
TCSC	40/ kVar controlled portions
STATCOM	50/kVar
UPFC series portions	50/kVar through power
UPFC shunt portions	50/kVar controlled

3. FACTS Devices

The development of FACTS devices in power transmission system has led to many applications of these controllers not only to improve various stability issues but also to provide operating flexibility to power systems. Although FACTS devices can offer high-speed control for enhancing the power system, one disadvantage of power electronics-based controllers is their high cost per unit of rating compared to similar conventional equipment [9]. However, the long list of benefits that these devices possess justifies their installation. Table I gives an idea about the cost of various FACTS controllers [9].

FACTS devices can be connected to a transmission line at any appropriate location in series, in shunt, or in a combination of series and shunt. SVC and STATCOM are connected in shunt, whereas TCSC and SSSC are connected in series. UPFC, on the other hand, is connected in series and shunt combination. Each of FACTS devices has its own characteristics and limitations. They are represented by different models and mathematical equations depending on the stability issue under consideration and the time frame involved. In the following subsections, the concepts and static models of all well-known FACTS devices are presented.

3.1. Shunt FACTS devices

3.1.1. SVC SVC is a shunt-connected static var generator/load whose output is adjusted to exchange capacitive or inductive current so as to maintain or control specific power system variables. SVC is similar to a synchronous condenser in that it is used to supply or absorb reactive power but without a rotating part. It contains an automatic voltage regulator system to set and maintain a target voltage level. The basic structure and terminal characteristic of SVC are shown in Figs 1 and 2, respectively. From Fig. 1, SVC is composed of a controllable shunt reactor and shunt capacitor(s). The total susceptance of an SVC can be controlled by controlling the firing angle of the thyristors. However, SVC acts like fixed capacitor or fixed inductor at the maximum and minimum limits, as shown in Fig. 2.

Appropriate model with DC representation of SVC can be incorporated in static voltage stability study by adding SVC equations in the power flow equations. The validated per-unit differential-algebraic equations (DAEs) corresponding to this model are as follows [16]:

$$\begin{bmatrix} \dot{x}_c \\ \dot{\alpha} \end{bmatrix} = f(x_c, \alpha, V, V_{\text{ref}}) \tag{3}$$

$$0 = \underbrace{\begin{bmatrix} B_e - \frac{2\alpha - \sin 2\alpha - \pi(2 - X_L/X_C)}{\pi X_L} \\ I - V_i B_e \\ Q - V_i^2 B_e \end{bmatrix}}_{g(\alpha, V, V_i, I, Q, B_e)} \tag{4}$$

where B_e is the total susceptance, α is firing angle of the thyristor, X_L is the inductance, X_C is the capacitance, I is the injected current, and V_i is the terminal voltage of SVC. Equation (4) can be introduced into the power flow equation in the CPF process. It

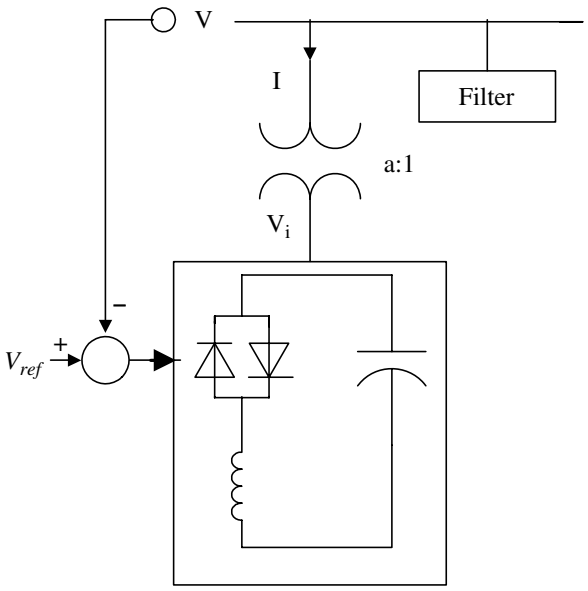

Fig. 1. Basic structure of SVC

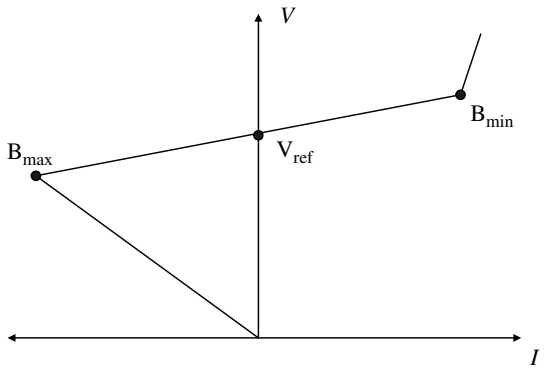

Fig. 2. Terminal characteristics of SVC

represents the limits not only on the firing angle α but also on the current I, the control voltage V, and the SVC voltage V_i, as well as the reactive power Q.

From Fig. 2 and (4), it can be observed that if SVC is represented only by an AC part, the behavior at the limits ($B_{\max}$, $B_{\min}$) can not be revealed. Moreover, the slope between $B_{\max}$ and $B_{\min}$ can be represented by the second subequation in (4).

3.1.2. STATCOM STATCOM is based on a solid-state synchronous voltage source and is analogous to an ideal synchronous machine except the rotating part. It generates a balanced set of sinusoidal voltages at the fundamental frequency with rapidly controllable amplitude and phase angle. As shown in Fig. 3, STATCOM is the voltage-source converter, which converts a DC input voltage into an AC output voltage in order to compensate for the active and reactive parts needed by the system. STATCOM could be viewed as superior to SVC because the former provides better terminal characteristics compared to diminishing characteristics at low terminal voltages by SVC. Figure 4 shows characteristic of STATCOM.

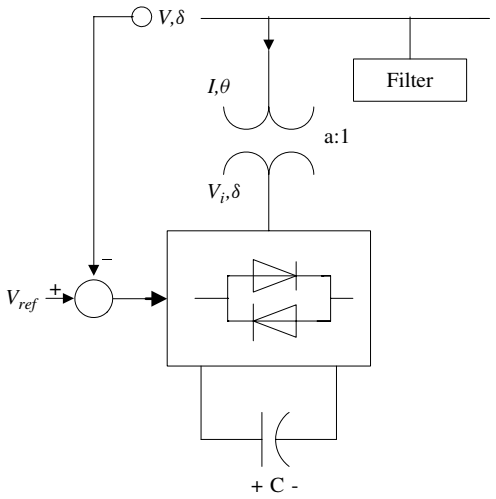

Fig. 3. Basic structure of STATCOM

The per-unit DAEs corresponding to STATCOM controller are described as follows:

$$\begin{bmatrix} \dot{x}_c \\ \dot{\alpha} \\ \dot{m} \end{bmatrix} = f(X_c, \alpha, m, V, V_{\rm dc}, V_{\rm ref}, V_{\rm dc,ref}) \tag{5}$$

$$\dot{V}_{\rm dc} = \frac{VI}{CV_{\rm dc}}\cos(\delta-\theta) - \frac{1}{R_c C}V_{\rm dc} - \frac{R}{C}\frac{I^2}{V_{\rm dc}} \tag{6}$$

$$0 = \underbrace{\begin{bmatrix} P - VI\cos(\delta-\theta) \\ Q - VI\sin(\delta-\theta) \\ P - V^2G + kV_{\rm dc}VG\cos(\delta-\alpha) + kV_{\rm dc}VB\sin(\delta-\alpha) \\ Q + V^2B - kV_{\rm dc}VB\cos(\delta-\alpha) + kV_{\rm dc}VG\sin(\delta-\alpha) \end{bmatrix}}_{g(\alpha,k,V,V_{dc},\delta,I,\theta,P,Q)} \tag{7}$$

where $V_{\rm dc}$ is DC voltage of voltage source inverter (VSI), m is modulation index, α is angle of internal synchronous voltage source, R_c is internal DC losses due to switching, X_c is reactance of the capacitor, δ is the angle of the voltage, and θ is the angle of the current.

The steady-state model of STATCOM can be readily obtained from (5)–(7) as

$$0 = \begin{bmatrix} V - V_{\rm ref} \pm X_{SL}I \\ V_{\rm dc} - V_{\rm dcref} \\ P - V_{\rm dc}^2/R_C - RI^2 \\ g(\alpha, k, V, V_{\rm dc}, \delta, I, \theta, P, Q) \end{bmatrix} \tag{8}$$

Equation (8) includes the AC and DC representation of STATCOM and it can be directly included in power flow program with the proper handling of limits to analyze the static voltage stability of a power system with STATCOM. If DC equations are introduced in the study, more practical solutions regarding to both AC and DC sides can be obtained.

3.2. Series FACTS devices

3.2.1. TCSC TCSC controllers use TCRs in parallel with segments of series capacitor bank. The combination of a TCR and capacitor allows the capacitive reactance to be smoothly controlled over a wide range and switched upon command to a condition where the bidirectional thyristor pairs conduct continuously and introduce appropriate reactance into the line. The basic structure of the device is shown in Fig. 5. The total susceptance of the line is controlled by controlling the firing angle of the thyristor.

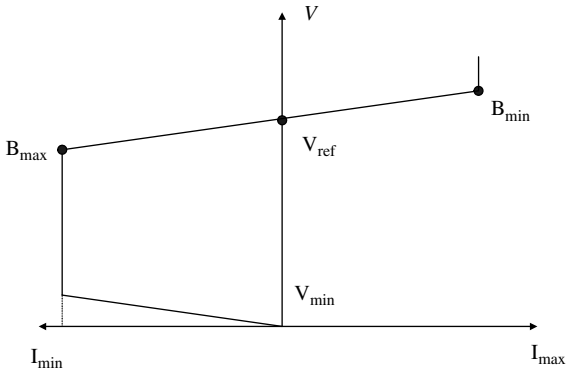

Fig. 4. Terminal characteristic of STATCOM

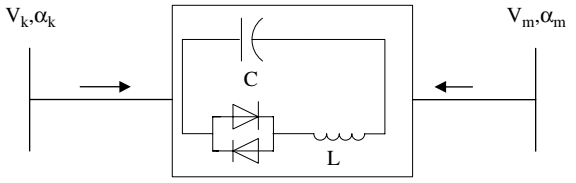

Fig. 5. Basic structure of TCSC

Suitable models to handle the control limits and operation constraints are important. The p.u. DAEs corresponding to this device are given as follows:

$$\begin{bmatrix} \dot{x}_c \\ \dot{\alpha} \end{bmatrix} = f(x_c, \alpha, V, V_{\rm ref}) \tag{9}$$

$$0 = \underbrace{\begin{bmatrix} P + V_k V_m B_e \sin(\delta_k - \delta_m) \\ -V_k^2 B_e + V_k V_m B_e \cos(\delta_k - \delta_m) - Q_k \\ -V_m^2 B_e + V_k V_m B_e \cos(\delta_k - \delta_m) - Q_m \\ B_e - B_e(\alpha) \\ \sqrt{P^2 + Q_k^2} - IV_k \end{bmatrix}}_{g(\alpha,V_k,V_m,\delta_k,\delta_m,I,P,Q_k,Q_m,B_e)} \tag{10}$$

where k and m are the buses where TCSC is connected in between,

$$\begin{aligned} B_e(\alpha) &= \pi(k_x^4 - 2k_x^2 + 1)\cos k_x(\pi-\alpha)/ \\ &\{X_C[\pi k_x^4 \cos k_x(\pi-\alpha) \\ &- \pi\cos k_x(\pi-\alpha) - 2k_x^4\alpha\cos k_x(\pi-\alpha) \\ &+ 2\alpha k_x^2\cos k_x(\pi-\alpha) - k_x^4\sin 2\alpha\cos k_x(\pi-\alpha) \\ &+ k_x^2\sin 2\alpha\cos k_x(\pi-\alpha) - 4k_x^3\cos^2\alpha\sin k_x(\pi-\alpha) \\ &- 4k_x^2\cos\alpha\sin\alpha\cos k_x(\pi-\alpha)]\} \end{aligned} \tag{11}$$

and

$$k_x = \sqrt{\frac{X_C}{X_L}} \tag{12}$$

The steady-state model of TCSC can be easily obtained from (10)–(12) as

$$0 = \begin{bmatrix} B_e - B_{e,\rm ref} \\ g(\alpha, V_k, V_m, \delta_k, \delta_m, I, P, Q_k, Q_m, B_e) \end{bmatrix} \tag{13}$$

which can be directly introduced into the power flow formulation. From (13), the total susceptance of TCSC can be controlled at a specific value.

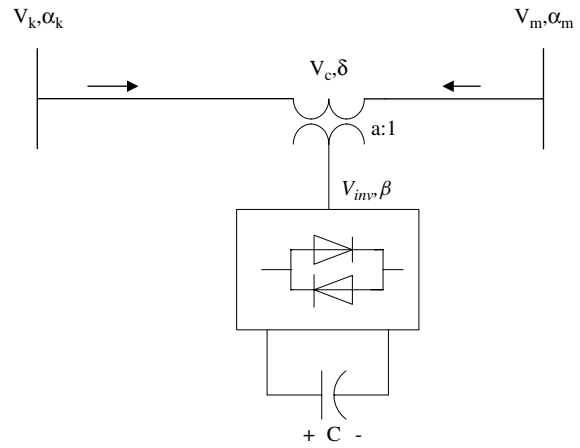

Fig. 6. Basic structure of SSSC

3.2.2. SSSC SSSC is based on a solid-state synchronous voltage source employing an appropriate DC-to-AC inverter with gate turn-off thyristor, which can be used for series compensation of transmission lines. SSSC is similar to STATCOM, as illustrated in Fig. 6, as it is based on a DC capacitor-fed VSI that generates a three-phase voltage at fundamental frequency, which is then injected into a transmission line through a transformer connected in series with the line.

The per-unit DAEs of SSSC including the control and operation limits can be elaborated as follows:

$$\begin{bmatrix} \dot{x}_c \\ \dot{\beta} \\ \dot{m} \end{bmatrix} = f(x_c, \beta, m, I, V_{\rm dc}, I_{\rm ref}, V_{\rm dcref}) \tag{14}$$

$$\dot{V}_{\rm dc} = \frac{VI}{CV_{\rm dc}}\cos(\delta-\theta) - \frac{G_C}{C}V_{\rm dc} - \frac{R}{C}\frac{I^2}{V_{\rm dc}} \tag{15}$$

$$0 = \underbrace{\begin{bmatrix} P_k - V_k I\cos(\delta_k-\theta) \\ Q_k - V_k I\sin(\delta_k-\theta) \\ P_m - V_m I\cos(\delta_m-\theta) \\ Q_m - V_m I\sin(\delta_m-\theta) \\ P - P_k + P_m \\ Q - Q_k + Q_m \\ P - V^2G + kV_{\rm dc}VG\cos(\delta-\beta) + kV_{\rm dc}VB\sin(\delta-\beta) \\ Q + V^2B - kV_{\rm dc}VB\cos(\delta-\beta) + kV_{\rm dc}VG\sin(\delta-\beta) \end{bmatrix}}_{g(\beta,k,V_{dc},V_k,V_m,V,\delta_k,\delta_m,\delta,I,\theta,P_k,P_m,P,Q_k,Q_m,Q)} \tag{16}$$

where β is angle of internal voltage, δ is angle of AC voltage generated by SSSC, and G_c is $1/R_c$.

To realize the models in power flow program, (14)–(16) are used as

$$0 = \begin{bmatrix} I - I_{\rm ref} \\ V_{\rm dc} - V_{\rm dcref} \\ P - G_C V_{\rm dc}^2 - RI^2 \\ g(\beta,k,V_{\rm dc},V_k,V_m,V,\delta_k,\delta_m,\delta,I,\theta,P_k,P_m,P,Q_k,Q_m,Q) \end{bmatrix} \tag{17}$$

which can be incorporated directly into the power flow program. DC equations are included in the formulation to provide more practical solutions on DC side.

3.3. UPFC UPFC consists of two identical VSIs: one in shunt and the other one in series with the line. Two inverters, namely, a shunt inverter and a series inverter, that operate via a common DC link with a DC storage capacitor allow the UPFC to independently control active and reactive power flows in the line as well as the bus voltage. Active power can freely flow in either direction between the AC terminals of the two inverters through the DC link. Although each inverter can generate or absorb reactive power at its own AC output terminal, it cannot internally exchange reactive power through DC link. The general scheme of UPFC is illustrated in Fig. 7.

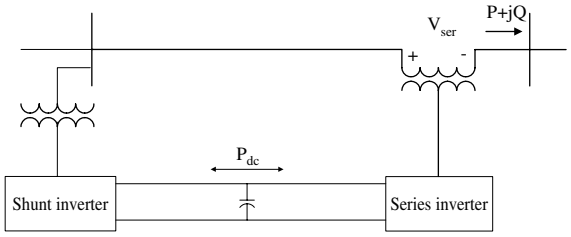

Fig. 7. UPFC configuration

It is obvious that the operation of UPFC is very important because it affects both the transmission line flow and voltage magnitude. Operation limit and control constraints of UPFC are very crucial to realize the actual operation of the device. To realize that, the validated per-unit DAEs corresponding to this model can be derived as follows:

$$\begin{bmatrix} \dot{x}_c \\ \dot{\alpha} \\ \dot{\beta} \\ \dot{m}_{sh} \\ \dot{m}_{se} \end{bmatrix} = f(x_c, \alpha, \beta, m_{sh}, m_{se}, V_k, V_l, V_{\rm dc}, \delta_k, \delta_l, P_{l,\rm ref}, Q_{l,\rm ref}, V_{k,\rm ref}, V_{\rm dc,ref}) \tag{18}$$

$$\dot{V}_{\rm dc} = \frac{V_k I_{sh}}{CV_{\rm dc}}\cos(\delta_k-\theta_{\rm sh}) + \frac{V_m I_l}{CV_{\rm dc}}\cos(\delta_m-\theta_l) - \frac{G_C}{C}V_{\rm dc} - \frac{R_{\rm sh}}{C}\frac{I_{\rm sh}^2}{V_{\rm dc}} - \frac{R_{\rm se}}{C}\frac{I_l^2}{V_{\rm dc}} \tag{19}$$

$$0 = \underbrace{\begin{bmatrix} P_{\rm sh} - V_k I_{\rm sh}\cos(\delta_k-\theta_{\rm sh}) \\ Q_{\rm sh} - V_k I_{\rm sh}\sin(\delta_k-\theta_{\rm sh}) \\ P_{\rm sh} - V_k^2 G_{\rm sh} + k_{\rm sh}V_{\rm dc}V_k G_{\rm sh}\cos(\delta_k-\alpha) \\ +k_{\rm sh}V_{\rm dc}V_k B_{\rm sh}\sin(\delta_k-\alpha) \\ Q_{\rm sh} + V_k^2 B_{\rm sh} - k_{\rm sh}V_{\rm dc}V_k B_{\rm sh}\cos(\delta_k-\alpha) \\ +k_{\rm sh}V_{\rm dc}V_k G_{\rm sh}\sin(\delta_k-\alpha) \end{bmatrix}}_{g_{sh}(\alpha,k_{sh},V_k,V_{\rm dc},\delta_k,I_{sh},\theta_{sh},P_{sh},Q_{sh})} \tag{20}$$

$$0 = \underbrace{\begin{bmatrix} P_k - P_{\rm sh} - V_k I_l\cos(\delta_k-\theta_l) \\ Q_k - Q_{\rm sh} - V_k I_l\sin(\delta_k-\theta_l) \\ P_l - V_m I_l\cos(\delta_m-\theta_l) \\ Q_l - V_m I_l\sin(\delta_m-\theta_l) \\ P_k - P_l - P_{\rm sh} - P_{\rm se} \\ Q_k - Q_l - Q_{\rm sh} - Q_{\rm se} \\ P_{\rm se} - V^2 G_{\rm se} + k_{\rm se}V_{\rm dc}VG_{\rm se}\cos(\delta-\beta) \\ +k_{\rm se}V_{\rm dc}VB_{\rm se}\sin(\delta-\beta) \\ Q_{\rm se} + V^2 B_{\rm se} - k_{\rm se}V_{\rm dc}VB_{\rm se}\cos(\delta-\beta) \\ +k_{\rm se}V_{\rm dc}VG_{\rm se}\sin(\delta-\beta) \end{bmatrix}}_{g_{se}(\beta,k_{se},V_{\rm dc},V_k,V_l,V,\delta_k,\delta_l,\delta,I_l,\theta_l,P_k,P_l,P_{sh},P_{se},Q_k,Q_l,Q_{sh},Q_{se})} \tag{21}$$

$$0 = \underbrace{\begin{bmatrix} I_k\cos(\theta_k) - I_{\rm sh}\cos(\theta_{\rm sh}) - I_l\cos(\theta_l) \\ I_k\sin(\theta_k) - I_{\rm sh}\sin(\theta_{\rm sh}) - I_l\sin(\theta_l) \\ P_k - V_k I_k\cos(\delta_k-\theta_k) \\ Q_k - V_k I_k\sin(\delta_k-\theta_k) \end{bmatrix}}_{g_{\rm con}(V_k,\delta_k,I_k,I_{sh},I_l,\theta_k,\theta_{sh},\theta_l,P_k,Q_k)} \tag{22}$$

where the subscripts se and sh represent series and shunt components, respectively, and l represents the line used for current and power flow control.

The UPFC steady-state model can be obtained by using (19)–(22) as

$$0 = \begin{bmatrix} V_k - V_{k,\mathrm{ref}} \\ V_{\mathrm{dc}} - V_{\mathrm{dc,ref}} \\ P_{\mathrm{se}} - P_{\mathrm{se,ref}} \\ Q_{\mathrm{se}} - Q_{\mathrm{se,ref}} \\ P_{\mathrm{sh}} - P_{\mathrm{se}} - G_C V_{\mathrm{dc}}^2 - R_{\mathrm{sh}} I_{\mathrm{sh}}^2 - R_{\mathrm{se}} I_l^2 \\ g_{\mathrm{sh}}(\alpha, k_{\mathrm{sh}}, V_k, V_{\mathrm{dc}}, \delta_k, I_{\mathrm{sh}}, \theta_{\mathrm{sh}}, P_{\mathrm{sh}}, Q_{\mathrm{sh}}) \\ g_{\mathrm{se}}(\beta, k_{\mathrm{se}}, V_{\mathrm{dc}}, V_k, V_l, V, \delta_k, \delta_l, \delta, I_l, \theta_l, P_k, P_l, \\ P_{\mathrm{sh}}, P_{\mathrm{se}}, Q_k, Q_l, Q_{\mathrm{sh}}, Q_{\mathrm{se}}) \\ g_{\mathrm{con}}(V_k, \delta_k, I_k, I_{\mathrm{sh}}, I_l, \theta_k, \theta_{\mathrm{sh}}, \theta_l, P_k, Q_k) \end{bmatrix} \tag{23}$$

which again can be incorporated into the power flow program.

The limits of UPFC can be divided into two limits: shunt compensation limits, and series compensation limit. Shunt compensation limits are basically the firing angle and V_{dc} limits, which can be handled in the same way as in the case of STATCOM. The series compensation limit, however, involves the capacity of the series compensation, which incorporates the active and reactive power limits.

AC/DC model including AC and DC equations of FACTS devices can be incorporated in the static voltage stability study by adding FACTS equations in the power flow equations. These models are used throughout this paper.

4. Placement and Sizing

Placement and sizing of FACTS devices are important issues. Placing FACTS devices with the appropriate sizes may enhance voltage stability of the system in an appropriate way. In this section, a new methodology is developed for placement of series FACTS devices and UPFC. Other methods are also available for placement and sizing, for each FACTS groups, namely, shunt, series, and combination.

4.1. Shunt FACTS

4.1.1. Placement The best location for reactive power compensation for improving static voltage stability margin is the 'weakest bus' of the system [14,17]. The weakest bus is defined as the one that is nearest to a bus experiencing voltage collapse and it can be found by using tangent vector in the predictor step of the CPF process. Introducing shunt FACTS device at the weakest bus will improve the voltage stability margin the most.

4.1.2. Suitable size In order to get a rough estimate of reactive power support needed at the weakest bus and corresponding LM for a given load and generation direction, a synchronous compensator with no limit on reactive power was used at the weakest bus. The amount of reactive generated at the maximum loading point from the synchronous compensator is considered as the suitable capacity of the shunt FACTS capacitors.

Another method of determining the capacities is to find the relationship between the maximum LF and the corresponding capacities that the devices can deliver without suffering from voltage collapse. The optimal capacity is found from the point at which there is no improvement in the LM.

4.2. Series FACTS

4.2.1. Placement One of the causes of voltage instability is the increase of reactive power losses that prevent sufficient reactive power supply from reaching the subregion needing the reactive power [2]. The reactive power loss sensitivity approach is proposed to narrow down the candidates and to identify the weakest line of the system. The weakest line is defined as a line that needs the reactive power the most. If the series compensation device is introduced at this line, the LM of the system will be increased to the maximum value.

Reactive power loss sensitivity (QLS or $\partial Q_{\mathrm{loss}}/\partial\lambda$) can be found by the ratio of the change of reactive power losses and the load increase. The equation of reactive power loss sensitivity or sensitivity index for placement is

$$\mathrm{QLS}_{ij} = \frac{\partial Q_{\mathrm{loss},ij}}{\partial\lambda} \approx \frac{\Delta Q_{\mathrm{loss},ij}}{\Delta\lambda} \tag{24}$$

where QLS_{ij} is the reactive power loss sensitivity on line ij,
$Q_{\mathrm{loss}_{,ij}}$ is the reactive power loss on line ij, and
λ is the load increase or LF.

Reactive power loss sensitivity can be written as a function of the sensitivity of the voltage to the load increase in (25). Sensitivity of voltage to the load increase ($\partial V/\partial\lambda$) is the tangent vector, which represents the weakest bus in the system. Thus, reactive power loss sensitivity can represent the weakest line of the system based on the location of the weakest bus.

$$\frac{\partial Q_{\mathrm{loss},ij}}{\partial\lambda} = \frac{\partial Q_{\mathrm{loss},ij}}{\partial V_i}\frac{\partial V_i}{\partial\lambda} + \frac{\partial Q_{\mathrm{loss},ij}}{\partial V_j}\frac{\partial V_j}{\partial\lambda} \tag{25}$$

where V_i and V_j are the voltage at the end of the line ij.

The sensitivity index is computed at the collapse point. The compensation device is located based on the sensitivity index, which identifies the location needing reactive power the most.

4.2.2. Suitable size The size of these series devices can be found by plotting the corresponding capacity of these devices against various LFs. The values of reactive power needed at the collapse point are the minimum capacity for the active and reactive power.

4.3. UPFC

4.3.1. Placement The best location for introducing UPFC controller can be found from a group of candidate locations of shunt and series compensation devices.

4.3.2. Suitable size The capacity of UPFC can be also found from the active and reactive power needed by the devices at the voltage collapse point. The capacities of shunt and series components are plotted separately. The reactive power requirements of shunt and series components at the collapse point constitute the capacity of UPFC.

5. Numerical Results

In this paper, sizing and placement techniques are proposed first to find the appropriate sizes and locations of FACTS devices for enhancing LM. Then, various performance measures of the system with FACTS devices including $P-V$ curves, voltage profiles, and power losses are investigated in normal and contingency conditions. LMs of the system with various FACTS devices are compared.

The IEEE 14-bus test system is used in the simulation, which consists of five synchronous machines including three synchronous compensators used only for reactive power support and two generators located at buses 1 and 2. In the system, there are 20 branches and 14 buses with 11 loads totaling 259 MW and 81.4 MVAr. The value of 259 MW is used as the base mega volt ampere (MVA) for load increase in the IEEE 14-bus test system. The modified IEEE 14-bus test system [4] is also used in this study. The modification from the original IEEE 14-bus test system

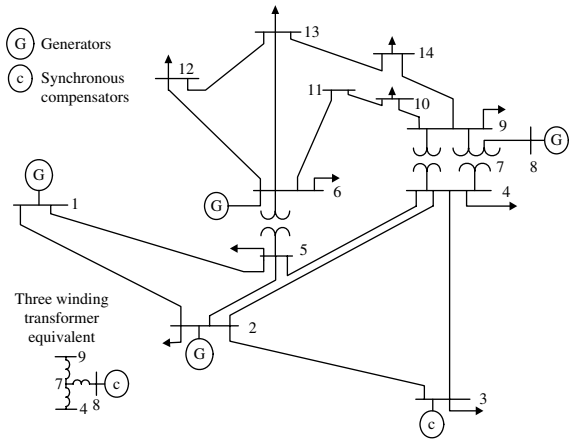

Fig. 8. Single-line diagram of the IEEE 14-bus test system

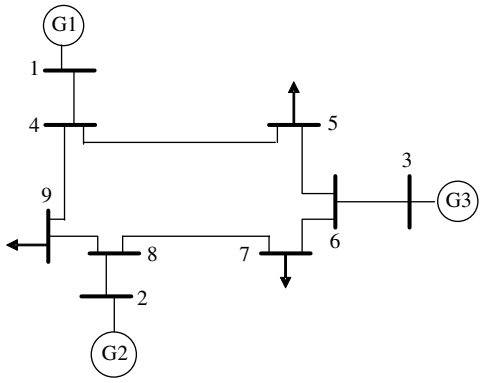

Fig. 9. Single-line diagram of the WSCC 9-bus test system

is that generators located at buses 6 and 8 were changed from synchronous compensators to generators. A single-line diagram of the modified IEEE 14-bus test system is depicted in Fig. 8.

The western systems coordinating council (WSCC) 9-bus test system is also used to validate the proposed method for placement of series FACTS devices and UPFC. The WSCC 9-bus test system consists of nine buses, three generators located at buses 1, 2, and 3, and three loads located at 5, 7, and 9. The total load in the system is 315 MW and 115 MVAr. Figure 9 shows the WSCC 9-bus test system.

The study is based on a program developed in MATLAB [18]. These programs are used to find the solution to the voltage stability study with FACTS devices. The result developed in MATLAB is compared with university of waterloo power flow (UWPFLOW) for the case of SVC, STATCOM, and TCSC. The UWPFLOW is a research tool that has been designed to calculate the LM of the power system for a given load and generation direction [17]. Only SVC, STATCOM, and TCSC are available in the UWPFLOW.

5.1. Placement and sizing of FACTS devices In order to simulate voltage stability based on CPF process, state variables of system with AC and DC representation of FACTS devices are introduced in the corrector and predictor steps in the numerical integration. The state variables of the system with SVC, STACOM, TCSC, SSSC, and UPFC are 33, 35, 36, 41, and 48, respectively. These state variables and FACTS equations were presented in Section 3.

5.1.1. Shunt FACTS devices The best location for reactive power compensation for improving static voltage stability margin is the "weakest bus" of the system [2,10,14]. The weakest bus is defined as the one that is nearest to experiencing the voltage collapse. The weakest bus of the system can be identified by using tangent vector analysis [2,10]. Tangent vector is the direction vector of the states on the system voltage profile. It is obtained from the predictor steps in the CPF process. In IEEE 14-bus test system, bus 14 is found to be the weakest bus.

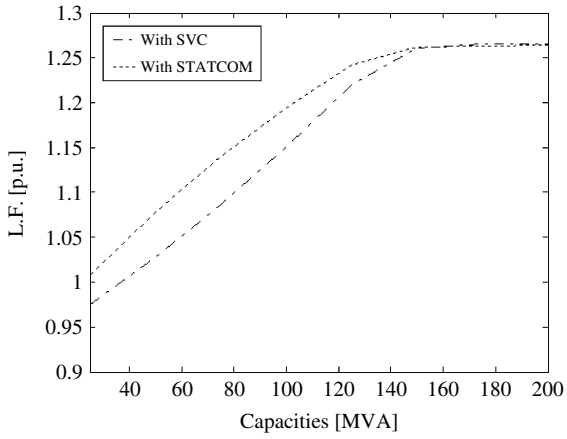

Fig. 10. Loading factor versus controller capacities for shunt FACTS devices

A method of determining the capacities is to find the relationship between the maximum LF and the corresponding capacities that the devices can deliver without voltage collapse [10]. These relationships for SVC and STATCOM are given in Fig. 10. It is clear from Fig. 10 that the optimum capacity required for both SVC and STATCOM is 150 MVAr. The voltage setting of these devices is 1.0 p.u. Voltage control is used for SVC and STATCOM.

Another sizing method is to introduce a synchronous compensator with no limit on reactive power at the weakest bus. The amount of reactive power generated at the maximum loading point from the synchronous compensator was found to be 150 MVAr at 1.0 p.u. voltage. This will be a good starting point of shunt FACTS capacities.

5.1.2. Series FACTS devices Reactive-power loss sensitivity approach is proposed to narrow down the candidates and to identify the weakest line of the system. The weakest line is defined as a line that needs the reactive power the most. If the series compensation device is introduced at this line, the LM of the system can be increased to the maximum value. Reactive-power loss sensitivity can be found by the ratio of the change of reactive power losses and the load increase. To validate the methodology and possibility for use in the power system applications, some simulations have been conducted in the test systems under various system conditions including stressed system conditions, which consider N-1 contingency in a transmission line.

The proposed method is at first validated in the WSCC 9-bus test system. Tables II and III show the reactive power loss sensitivity index ($\partial Q_{\text{loss}}/\partial\lambda$) near LM in the normal condition and N-1 condition at line 4–5, respectively. The N-1 line contingency of line 4–5 is arbitrarily selected as it is inside the main loop network of the system. The value in parenthesis represent ranking of the lines. The increase of reactive power losses (ΔQ_{loss}) is computed first by using load flow calculation at two LFs near the collapse point. Then, the reactive power loss sensitivity is calculated from the ratio of the increase of reactive power losses (ΔQ_{loss}) and the increase of LF ($\Delta\lambda$) as given by (24). LM with TCSC is obtained from $P-V$ curves using CPF analysis when TCSC is connected in the line shown in the leftmost column of the table. From Table II, the reactive power loss sensitivity (QLS) of line 4–9 is highest; placing the TCSC at this line would increase LM of the system the most. This can be seen from the LM results which show the highest LM when a TCSC is connected at line 4–9.

Table II. Reactive power loss sensitivity index near LM of WSCC 9-bus test systems in normal condition

Line	Normal condition of WSCC 9-bus test system		
	ΔQ_{loss} [MVAr] (ranking)	$\partial Q_{\text{loss}}/\partial\lambda$ [MVAr/p.u.] (ranking)	LM [p.u.] with TCSC (ranking)
4–9	7.400 (1)	1762 (1)	1.4783 (1)
4–5	3.940 (2)	938 (2)	1.2888 (2)
5–6	1.300 (5)	310 (5)	1.1209 (6)
6–7	2.370 (3)	564 (3)	1.1988 (4)
7–8	2.160 (4)	514 (4)	1.2050 (3)
8–9	1.200 (6)	286 (6)	1.1329 (5)

LM of base case without TCSC is 1.1543 p.u. There are six lines in the base case. The weakest bus is located at bus 9 and then changed to bus 4 near the collapse point.

Table III. Reactive power loss sensitivity index near LM of WSCC 9-bus test systems with N-1 contingency at line 4–5 in normal condition

Line	N-1 contingency of WSCC 9-bus test system		
	ΔQ_{loss} [MVAr] (ranking)	$\partial Q_{\text{loss}}/\partial\lambda$ [MVAr/p.u.] (ranking)	LM [p.u.] with TCSC (ranking)
4–9	0.820 (3)	804 (3)	0.5115 (3)
4–5	NA	NA	NA
5–6	3.440 (1)	3373 (1)	0.6561 (1)
6–7	0.300 (4)	294 (4)	0.4643 (4)
7–8	1.020 (2)	1000 (2)	0.5773 (2)
8–9	0.290 (5)	284 (5)	0.4522 (5)

LM of base case is 0.47802 p.u./ There are five lines in the base case./ The weakest bus is located at bus 5. NA is for the base case.

Table III shows the N-1 contingency case when the line 4–5 is disconnected. QLS at line 5–6 is the highest in this case; locating TCSC at this line increases LM of the system to the maximum value. Reactive power delivered by TCSC is calculated by using steady-state equations described in Section 3.

To further verify the effectiveness of the proposed method, the results of line ranking according to reactive power loss sensitivity ($\partial Q_{\text{loss}}/\partial\lambda$) for the IEEE 14-bus system and the modified IEEE 14-bus test system are shown in Tables IV and V and Tables VI and VII for the cases of normal condition and N-1 contingency at line 2–3, respectively. From Table IV, it can be noticed that lines 1–5 and 1–2 require the reactive power compensation the most, as they has the highest sensitivity $\partial Q_{\text{loss}}/\partial\lambda$. Having TCSC connected in lines 1–5 or 1–2 would increase LM to the maximum amount compared to the other cases. From Table V, connecting TCSC at line 3–4 in case of N-1 contingency at line 2–3 would result in the maximum LM.

For the modified IEEE 14-bus test system, QLS at lines 1–2 and 1–5 are the highest. Having TCSC at these lines provides the highest LM for this case. The QLS at line 1–2 is slightly higher than that at line 1–5 in this case. This is because introducing generation at bus 6 in the modified IEEE 14-bus system largely reduces reactive power losses at line 1–5. However, the rate of change of QLS at line 1–5 is higher compared to that at line 1–2. At the point very close to the collapse point, QLS of these two lines are identical. In this case, two possible locations, lines 1–2 and 1–5, should be considered. Table VII shows the modified test system with N-1 contingency. QLS at line 3–4 in this case is the highest, and introducing TCSC in this line enhances LM of the system the most.

From Tables II–VII, it is obvious that the reactive power loss sensitivity method offers close results in ranking the lines in terms of weakness compared to the case with TCSC, both in normal and

Table IV. Reactive power loss sensitivity index near LM of IEEE 14-bus test systems in normal condition

Line	Normal condition of IEEE 14-bus test system		
	ΔQ_{loss} [MVAr] (ranking)	$\partial Q_{\text{loss}}/\partial\lambda$ [MVAr/p.u.] (ranking)	LM [p.u.] with TCSC (ranking)
1–2	2.430 (2)	810 (2)	0.93501 (2)
1–5	2.480 (1)	827 (1)	1.00520 (1)
2–3	1.750 (3)	583 (3)	0.84004 (3)
2–4	1.170 (4)	390 (4)	0.75681 (4)
2–5	0.730 (5)	243 (5)	0.73623 (5)
3–4	0.190 (7)	63 (7)	0.71908 (7)
4–5	0.270 (6)	90 (6)	0.72798 (6)

LM of base case is 0.70398 p.u. There are 17 lines in the base case. The weakest bus is located at bus 14.

Table V. Reactive power loss sensitivity index near LM of IEEE 14-bus test system with N-1 contingency at line 2–3

Line	N-1 contingency of IEEE 14-bus test system		
	ΔQ_{loss} [MVAr] (ranking)	$\partial Q_{\text{loss}}/\partial\lambda$ [MVAr/p.u.] (ranking)	LM [p.u.] with TCSC (ranking)
1–2	0.440 (4)	151 (4)	0.32999 (4)
1–5	0.800 (2)	274 (2)	0.40591 (2)
2–3	NA	NA	NA
2–4	0.670 (3)	229 (3)	0.33042 (3)
2–5	0.360 (5)	123 (5)	0.29126 (6)
3–4	1.120 (1)	384 (1)	0.45186 (1)
4–5	0.210 (6)	72 (6)	0.29590 (5)

LM of base case is 0.24292 p.u. There are 16 lines in the base case. The weakest bus is located at bus 3. NA is for the base case.

Table VI. Reactive power loss sensitivity index near LM of the modified IEEE 14-bus test systems in normal condition

Line	Normal condition of modified IEEE 14-bus test system		
	ΔQ_{loss} [MVAr] (ranking)	$\partial Q_{\text{loss}}/\partial\lambda$ [MVAr/p.u.] (ranking)	LM [p.u.] with TCSC (ranking)
1–2	1.790 (1)	2797 (1)	1.1490 (2)
1–5	1.680 (2)	2625 (2)	1.2049 (1)
2–3	1.459 (3)	2279 (3)	1.0717 (3)
2–4	0.769 (4)	1201 (4)	0.96176 (4)
2–5	0.449 (5)	701 (5)	0.93838 (6)
3–4	0.223 (6)	349 (6)	0.93532 (7)
4–5	0.210 (7)	329 (7)	0.93844 (5)

LM of base case is 0.91064 p.u. There are 17 lines in the base case. The weakest bus is located at bus 14.

Table VII. Reactive power loss sensitivity index near LM of the modified IEEE 14-bus test system with N-1 contingency at line 2–3

Line	N-1 contingency of the modified IEEE 14-bus test system		
	ΔQ_{loss} [MVAr] (ranking)	$\partial Q_{\text{loss}}/\partial\lambda$ [MVAr/p.u.] (ranking)	LM [p.u.] with TCSC (ranking)
1–2	1.130 (4)	408 (4)	0.43412 (4)
1–5	1.970 (2)	711 (2)	0.50519 (2)
2–3	NA	NA	NA
2–4	1.770 (3)	639 (3)	0.44284 (3)
2–5	0.880 (5)	318 (5)	0.40278 (6)
3–4	4.860 (1)	1755 (1)	0.64573 (1)
4–5	0.690 (6)	249 (6)	0.41532 (5)

LM of base case is 0.37277 p.u. There are 16 lines in the base case. The weakest bus is located at bus 3. NA is for the base case.

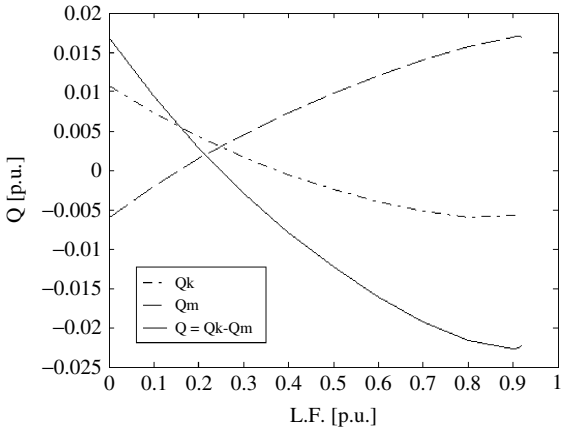

Fig. 11. Capacity of TCSC at various LFs

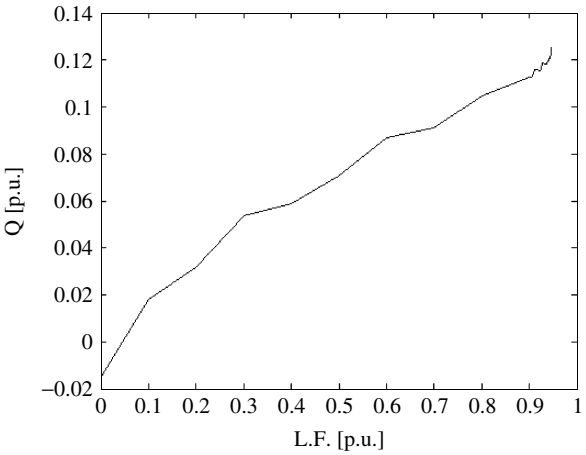

Fig. 12. Reactive power capacity of SSSC at various LFs

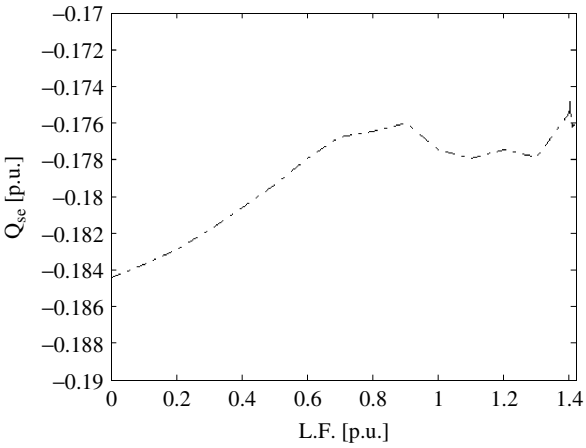

Fig. 13. Q_{se} of UPFC at various LFs

in contingency conditions. However, in the modified IEEE 14-bus test system, there is one incorrect ranking in the first position in the normal case due to close values of LM. Changing the synchronous condenser to generator at bus 6 largely reduces reactive power flow in the line 1–5. However, a group of candidate buses having high reactive power loss sensitivity could be considered. According to this, the reactive power sensitivity method provides an effective method not only to identify the weakest line but also to rank the lines in terms of reactive power losses.

The reactive power loss sensitivity index is computed close to the collapse point. The compensation device is located based on the index, which identifies the location needing reactive power the most. The index is sensitive to contingencies, as the power system network is changed when contingency occurred. The criterions for the use of the index depend upon operating condition, i.e. normal or contingency, defined by utilities. If the contingency is occurred at FACTS devices, the worst situation may happen. In this study, N-1 contingency of shunt FACTS devices is the base case as the system is returned to the intact case. The N-1 contingency of series FACTS devices and UPFC is the N-1 of the line where series FACTS devices or UPFC is connected.

Since TCSC at line 1–5 increases the LM the most in normal condition, in the rest of the study the series FACTS devices are placed at line 1–5. The modified IEEE 14-bus test system [4] is used for the rest of the study.

Sizing of TCSC and SSSC can be found from the voltage stability study. The size of these series devices can be found by plotting the corresponding capacity of these devices against various LFs. For TCSC, Fig. 11 shows the capacity of Q_k reactive power delivered at the sending bus, Q_m reactive power absorbed at the receiving bus, and Q reactive power delivered/absorbed by TCSC with respect to LFs. The base value of real and reactive power of FACTS devices in the study is 100 MVA. From Fig. 11, at the collapse point, TCSC delivers reactive power about 2.4 MVAr. Hence, the value of 2.4 MVAr is used as the capacity of TCSC. In the base case, real and reactive power flows in line 1–5 are 0.3838 and 0.05 p.u., respectively.

Figure 12 shows the corresponding reactive power capacities of SSSC at various LFs. From Fig. 12, at the collapse point, SSSC delivers reactive power about 12.5 MVAr. From the simulation, active power needed by SSSC at the collapse point is 0.2 MW. These values are used for the active and reactive power capacity of SSSC.

5.1.3. UPFC devices The best location for introducing UPFC controller can be found from a group of candidate locations of shunt and series compensation devices. From the group of candidate buses, it was found that, for the modified IEEE 14-bus test system, UPFC should be placed at line 9–14 to have the highest LM. Line 9–14 is one of candidate locations of shunt FACTS device since it is the line connected to the weakest bus, i.e. bus 14.

The capacity of UPFC can be also found from the active and reactive power needed by the devices at the collapse point. The capacities of shunt and series component are plotted separately. From the simulation, active power required at the collapse point for series and shunt components are 0.45 and 2.3 MW, respectively. Figures 13 and 14 show the reactive power needed by series and shunt components of UPFC, respectively. From these figures, it can be seen that highest reactive power requirement are 18.4 and 100 MVAr for series and shunt components, respectively. The capacity of UPFC is much lower than that of STATCOM, which is 150 MVAr. In practice, the parameters of FACTS devices including capacities, reactance, etc., should be selected based on the available sizes in the market. The variations in the Figs 12 and 13 are due to numerical nature when the value is small.

5.2. P–*V* curves and voltage profiles In this section, various FACTS controllers are compared. Figure 15 shows P–V curves of the base case with FACTS devices for the modified IEEE 14-bus test system. LM of the base case and various FACTS devices are shown in Table VIII. From Fig. 15 and Table VIII, it can be observed that UPFC gives the highest LM improvement followed by shunt FACTS devices and series FACTS devices. The modified IEEE 14-bus test system requires reactive power compensation at the distribution level; therefore installing shunt reactive devices could provide higher LM than series devices. The UPFC, on the other hand, is composed of both shunt and series

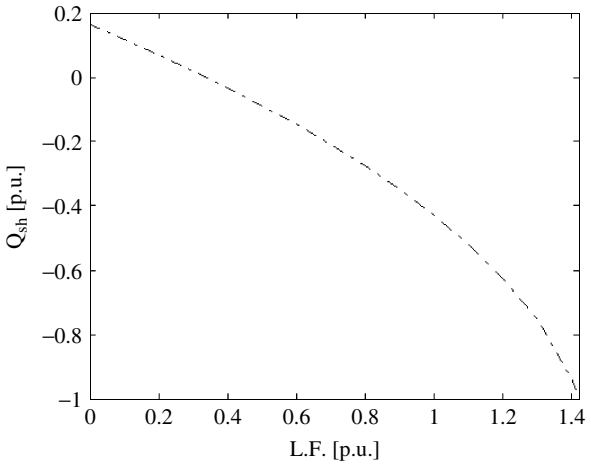

Fig. 14. Q_{sh} of UPFC at various LFs

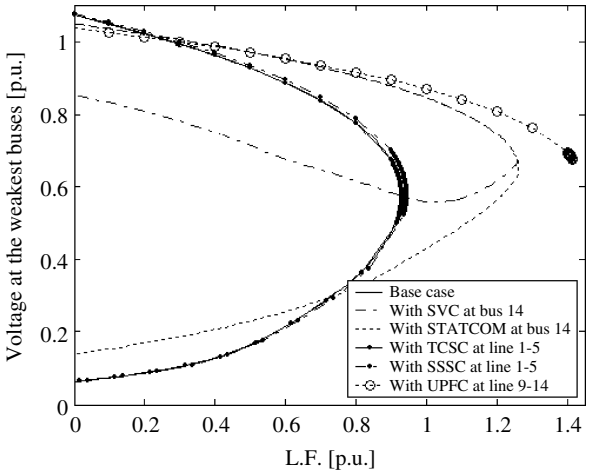

Fig. 15. $P-V$ curves of the base case and the cases with FACTS devices

Table VIII. LM and percentage increase of LM of base case, with FACTS devices

Case	LM [p.u]	LM increase	% Increase
Base case	0.9278	NA	NA
SVC	1.2606	0.3328	35.9
STATCOM	1.2625	0.3347	36.1
TCSC	0.9307	0.0029	0.3
SSSC	0.9452	0.0174	1.9
UPFC	1.4165	0.4887	52.7

NA is for the case without FACTS devices.

devices. Introducing UPFC can provide reactive power both at the bus and at the line, thus making the device the most effective one in terms of LM improvement in this test system.

Voltage profiles close to the collapse point of base case with and without FACTS devices are illustrated in Fig. 16. From Fig. 16, it can be seen that UPFC provides better voltage profiles than other FACTS devices. Compared to series FACTS devices, shunt devices give better voltage profiles since the reactive power is introduced at the weakest bus.

5.3. Power losses Total real and reactive power losses of the system are plotted in Figs 17 and 18, respectively. From the figures, it can be seen that both real and reactive power losses follow the same pattern against load increase. The UPFC results

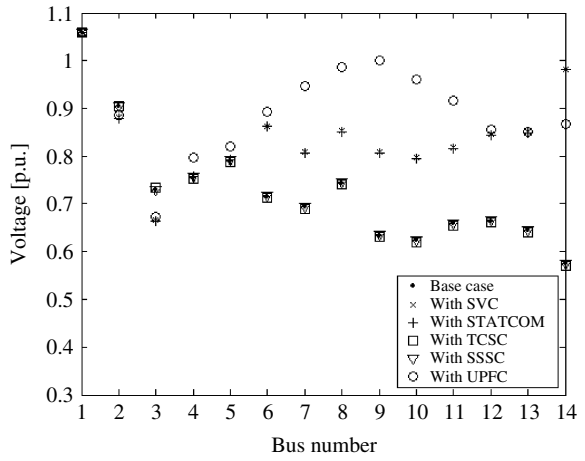

Fig. 16. Voltage profile of the base case and the cases with FACTS devices

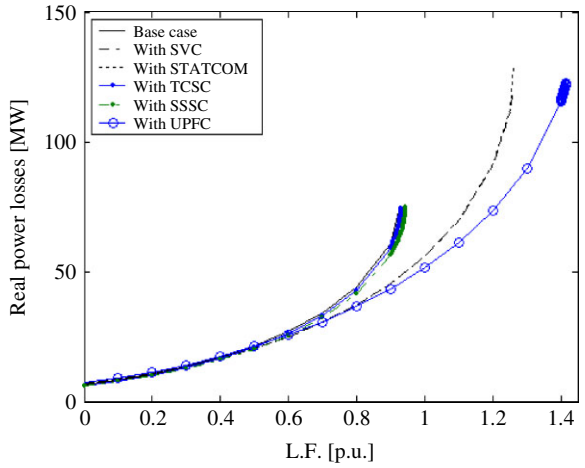

Fig. 17. Real power losses of the system with FACTS devices

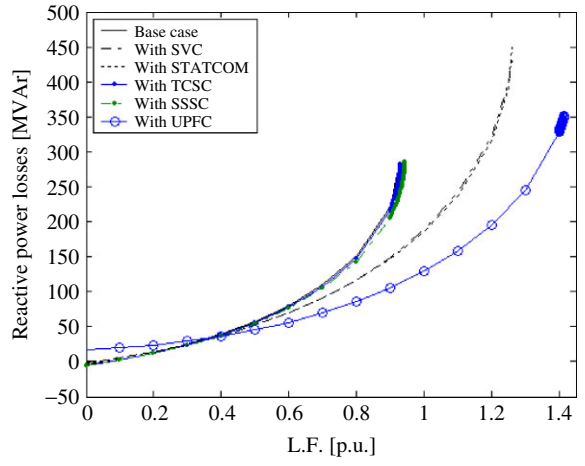

Fig. 18. Reactive power losses of the system with FACTS devices

in the lowest losses as well as the incremental losses compared to other FACTS devices, thus giving highest LM and better voltage profile. Shunt FACT devices provide lower losses compared to series FACTS devices.

5.4. Contingencies Comparison of LMs for three worst contingency cases is shown in Table IX for various FACTS devices. Shunt FACTS devices provide higher LM than series

Table IX. Loading margin for various line outages for base case and the cases with various FACTS controllers

Case	Loading margins [p.u.] for line outages		
	1-2	2-3	1-5
Without FACTS	0.25184	0.38278	0.59605
SVC	0.40205	0.49212	0.87061
STATCOM	0.40097	0.49174	0.86916
TCSC	NA	0.4033	NA
SSSC	NA	0.3964	NA
UPFC	0.5003	0.5596	1.0161

Table X. Capacity, LM, cost, LMIC, and ranking for all FACTS devices

FACTS	Capacity [MVA] (shunt, series)	LM [p.u.]	Cost [million USD]	LMIC [p.u./ USD]	Ranking
SVC	(150, 0)	0.3328	6	5.54667E−08	2
STATCOM	(150, 0)	0.3347	7.5	4.46267E−08	3
TCSC	(0, 2.4)	0.0029	0.096	3.02083E−08	4
SSSC	(0, 12.5)	0.0174	0.625	2.784E−08	5
UPFC	(100, 18.4)	0.4887	5.92	8.25507E−08	1

NA is for the unstable case.

FACTS devices for all contingency cases, as the system requires reactive power to compensate the reactive power load. UPFC is the device that gives the highest improvement in voltage stability margin. The N-1 contingency of SVC and STATCOM is the intact case with 0.91064 LM in p.u. For the N-1 contingency of TCSC, SSSC, and UPFC, the LM of the system is 0.76781 p.u.

5.5. Loading margin increase per cost In order to compare technical merits and cost of FACTS devices, LM increase per cost (LMIC) is proposed based on the ratio of the increase of loadability and the cost. Table X shows capacity, LM, cost, LMIC, and ranking for all FACTS devices with the capacity obtained from the previous Sections. From the table, it is concluded that UPFC has the highest LMIC followed by SVC, STATCOM, TCSC, and SSSC, respectively. Having UPFC installed in the system may be the most beneficial to the system in terms of LM and investment cost.

6. Conclusion

A comprehensive comparison of five well-known FACTS devices for loadability enhancement was presented in this paper. A sensitivity factor based technique for series FACTS devices was also proposed for static voltage stability improvement.

Detailed numerical results obtained for modified IEEE 14-bus test system showed that UPFC gives the highest LMs in all the cases, including contingency cases. UPFC also results in lower real and reactive power losses and better voltage profile at different loading conditions. Results also showed that shunt FACTS devices are better than their series counterpart in enhancing loadability in the intact and contingency conditions. This group of FACTS devices also yields low loss and better voltage profile compared to series FACTS devices. Both shunt devices, i.e. SVC and STATCOM, show comparable performance, and series devices too show comparable performance, for different operating conditions. However, the VSC-based FACTS devices show a slightly better performance in series and shunt groups compared to the respective traditional FACTS device.

Acknowledgments

This work was supported by the Thailand Research Fund (TRF) under Grant MRG5080412.

References

(1) Kundur P. *Power System Stability and Control.* McGrawHil: 1994.
(2) IEEE/PES Power System Stability Subcommittee. *Voltage Stability Assessment: Concepts, Practices and Tools*, special publication, final draft, 2003.
(3) Blackout of 2003. *Description and Responses*. http://www.pserc.wisc.edu/. Accessed November, 2009.
(4) Sode-Yome A, Mithulananthan N, Lee KY. A maximum loading margin method for static voltage stability in power systems. *IEEE Transactions on Power Systems* 2006; **21**:799–808.
(5) Sode-Yome A, Mithulananthan N. Maximizing static voltage stability margin in power systems using a new generation pattern. *Australian Journal of Electrical and Electronics Engineering* 2005; **2**(**3**):255–261.
(6) Sode-Yome A, Mithulananthan N. An economical generation direction for power system static voltage stability. *Electric Power System Research Journal* 2006; **76**(**12**):1075–1083.
(7) Canizares CA, De Souza ACZ, Quintana VH. Comparison of performance indices for detection of proximity to voltage collapse. *IEEE Transactions on Power Systems* 1996; **11**(**3**):1441–1447.
(8) Lee BH, Lee KY. Dynamic and static voltage stability enhancement of power systems. *IEEE Transactions on Power Systems* 1993; **8**(**1**):231–238.
(9) Cigre 95 TP108. *FACTS Overview*. IEEE Power Engineering Society, 1995.
(10) Sode-Yome A, Mithulananthan N. Comparison of shunt capacitor, SVC and STATCOM in static voltage stability margin enhancement. *International Journal of Electrical Engineering Education, UMIST* 2004; **41**(**3**):158–171.
(11) Canizares CA. Power flow and transient stability models of FACTS controllers for voltage and angle stability studies. *IEEE/PES Winter Meeting on Modeling, Simulation and Applications of FACTS Controllers in Angle and Voltage Stability Studies*, Singapore, 2000.
(12) Farsangi MM, Song YH, Lee KY. Choice of FACTS device control inputs for damping inter-area oscillations. *IEEE Transactions on Power Systems* 2004; **19**(**2**):1135–1143.
(13) Farsangi MM, Nezamabadi-Pour H, Song YH, Lee KY. Placement of SVCs and selection of stabilizing signals for in power systems. *IEEE Transactions on Power Systems* 2007; **22**(**3**):1061–1071.
(14) Canizares CA, Faur ZT. Analysis of SVC and TCSC controllers in voltage collapse. *IEEE Transactions on Power Systems* 1999; **14**(**1**):158–165.
(15) Canizares CA, Uzunovic E, Reeve J, Johnson BK. *Transient Stability and Power Flow Models of the Unified Power Flow Controller for Various Control Strategies.* Technical Report 2004-9, University of Waterloo: Waterloo, 2004.
(16) Uzunovic E, Canizares CA, Reeve J. Fundamental frequency model of unified power flow controller. *Proceedings of the North American Power Symposium (NAPS)*, Cleveland, Ohio, 1998; 294–299.
(17) Cañizares CA, Alvarado FL, Zhang S, Watson M. UWPFLOW. *Continuation and Direct Methods to Locate Fold Bifurcations in AC/DC/FACTS Power Systems*, University of Waterloo, 2004. http://www.power.uwaterloo.ca. Accessed November, 2009.
(18) MATLAB Functions. 2004, http://www.mathworks.com. Accessed November, 2009.

Appendix

Table A1. SVC data

X_c (p.u.)	X_l (p.u.)	α_{min} (°C)	α_{max} (°C)	Slope (%)	S (MVA)	kV
1.1708	0.4925	90	175	2	150	26

Table A2. STATCOM data

R_c (p.u.)	R (p.u.)	X (p.u.)	S (MVA)	k	X_{sl} (%)
0.0017	0	0.145	150	0.9	2

Table A3. TCSC data

X_c (p.u.)	X_l (p.u.)	α_{min} (°C)	α_{max}(°C)	S (MVA)
10% of X_l	50% of the line	144	175	100

Table A4. SSSC data

R_c (p.u.)	R (p.u.)	X (p.u.)	S (MVA)	K
0.0017	0	0.145	100	0.9

Table A5. UPFC data: shunt part

R_c (p.u.)	R (p.u.)	X (p.u.)	S (MVA)	K	X_{sl} (%)
0.0017	0	0.145	150	0.9	2

Table A6. UPFC data: series part

R_c (p.u.)	R (p.u.)	X (p.u.)	S (MVA)	k
0.0017	0	0.145	100	0.9

Arthit Sode-Yome (Non-member) received the B.Eng. degree from the Prince of Songkla University, Thailand, in 1993, the M.S. degree from the Pennsylvania State University, USA, in 1996, both in electrical engineering, and the Ph.D. degree in energy from the Asian Institute of Technology, Thailand, in 2005. He is currently a Lecturer with the Department of Electrical Engineering, Siam University, Thailand. His main research interests include voltage stability, FACTS, neural networks, optimization techniques, and HVDC.

Nadarajah Mithulananathan (Non-member) received the Ph.D. degree from University of Waterloo, Canada, in electrical and computer engineering in 2002. He worked as an electrical engineer with the Generation Planning Branch of Ceylon Electricity Board in Srilanka and as a Researcher at Chulalongkorn University, Bangkok, Thailand. He is currently a Senior Lecturer at the University of Queensland, Australia. He has also served as an Associate Professor with the Asian Institute of Technology, Bangkok, Thailand. His main research interests include voltage stability and oscillation studies on practical power systems, application of FACTS controllers, and renewable energy technology.

KwangY. Lee (Non-member) received the B.S. degree from the Seoul National University, Korea, in 1964, the M.S. degree from North Dakota State University, Fargo, USA, in 1968, both in electrical engineering, and the Ph.D. degree in systems science from Michigan State University, East Lansing, USA, in 1971. He has been on the faculties of Michigan State University, Oregon State University, Houston University, the Pennsylvania State University, and Baylor University, USA, where he is currently Professor and Chair of Electrical and Computer Engineering and Director of Power and Energy Systems Laboratory. His research interests include power systems control, operation and planning, and intelligent systems applications to power plants, and power systems control. Dr Lee is a Fellow of IEEE, Editor of *IEEE Transactions on Energy Conversion*, and former Associate Editor of *IEEE Transactions on Neural Networks*.